Supplementary Information

Interface engineering of MnO_2 for high-performance photo-rechargeable Zn ion batteries

Ting Xiong[a,*] Chen Xin[a], Dan Yang[a], Wenzhan Zhang[a], Hua-Kun Liu[a]

[a] Institute of Energy Materials Science (IEMS), University of Shanghai for Science and Technology, Shanghai 200093, China. [*]Correspondence: txiong@usst.edu.cn.

EXPERIMENTS

Synthesis of MnO_2

In a standard synthesis, an aqueous solution of $MnSO_4 \cdot 5H_2O$ (0.1 M, 50 mL) was combined with an equal volume of $K_2S_2O_8$ (0.1 M, 50 mL). Subsequently, NaOH solution (1.2 M, 25 mL) was introduced into the mixture. The resulting suspension was then divided between two 100 mL Teflon-lined autoclaves and subjected to hydrothermal treatment at 160 °C for 24 hours.

Synthesis of TiO_2@Ti

The cleaned Ti mesh was placed in a muffle furnace and calcined at 400 °C for 1 h to obtain a TiO_2@Ti mesh.

Characterization

The morphology and microstructure were examined by scanning electron microscopy (SEM, ZEISS Sigma 360) coupled with energy-dispersive X-ray spectroscopy (EDS), as well as by transmission electron microscopy (TEM, Thermo Talos F200X). The crystal structure and phase composition were determined by X-ray powder diffraction (XRD, DX-27 mini) using Cu Kα radiation. Optical properties were investigated by UV–Vis diffuse reflectance spectroscopy (UV–Vis DRS, Shimadzu UV-3600). The Ultraviolet photoelectron spectroscopy (UPS) was measured using Thermo SCIENTIFIC Nexsa.

Electrochemical Measurements

MnO_2 powder was employed directly as the active material. A slurry was prepared by thoroughly mixing the constituent powders in a weight ratio of 7:2:1 for MoS_2, carbon black, and polyvinylidene fluoride in N-methyl-2-pyrrolidone solvent. This slurry was subsequently coated onto a TiO_2@Ti mesh and dried at 70 °C to form the MnO_2-based photocathode. Coin-type cells (perforated CR2032) were assembled using the as-prepared MnO_2/TiO_2@Ti as the photocathode, a glass fiber membrane as the separator, a zinc foil as the anode, and an aqueous electrolyte consisting of 2 M $ZnSO_4$ and 0.2 M $MnSO_4$. The perforated window of the coin cell was sealed with transparent 3M VHB adhesive tape to allow light illumination. For flexible device fabrication, the

components were encapsulated in a transparent polymer pouch.

All electrochemical measurements were performed using a Bio-logic EC-Lab VMP3 potentiostat under controlled conditions (25 °C, 40% relative humidity). The operating voltage window was set between 1.0 and 1.8 V. Cyclic voltammetry (CV) was conducted at scan rates ranging from 0.2 to 2.0 mV s^{-1}, while galvanostatic charge/discharge (GCD) tests were carried out at current densities from 0.2 to 2 A g^{-1}. Electrochemical impedance spectroscopy (EIS) was measured in the frequency range of 0.1 Hz to 10^5 Hz. For photo-electrochemical characterization, a 100 W xenon lamp equipped with a 420 nm cutoff filter was used to provide visible-light irradiation (light intensity: 20 mW cm^{-2}). In photo-charging experiments, the cell was first discharged to a defined state, followed by open-circuit charging under illumination without any applied electrical bias. Photocurrent responses of the MnO_2/TiO_2@Ti and control MnO_2@Ti electrodes were recorded in a three-electrode configuration using 0.5 M Na_2SO_4 electrolyte under chopped illumination (30 s light on/off cycles) at open-circuit potential.

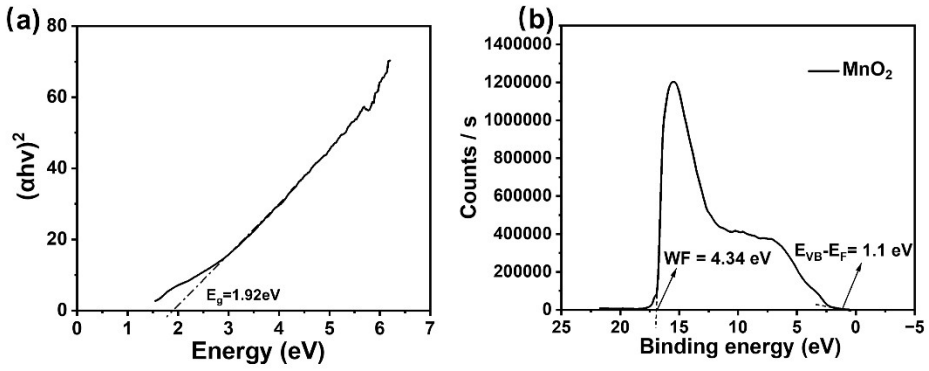

Fig. S1 (a) Tauc plot of MnO_2 (E_g: the optical band gap), (b) The UPS of MnO_2 with Ag as a reference (WF: Work Function; E_{VB}: Valence Band Maximum; E_f: Fermi Level).

Based on the UPS spectrum shown in Fig. S1b, the work function (φ) of MnO_2 is determined to be 4.34 eV, calculated using the equation φ = 21.22 eV − 16.88 eV. Consequently, the Fermi level (E_F) of MnO_2 is estimated to be −0.1 V vs. NHE (SHE), derived from the relationship E_F (V vs. NHE) = −4.44 eV + φ (eV). Furthermore, the energy difference between the Fermi level and the valence band maximum is found to be 1.1 eV, which is obtained by extrapolating the linear portion of the low binding-energy cutoff in the UPS spectrum to the baseline. Based on this value, the valence band potential (E_{VB}) is calculated to be 1.0 V vs. NHE. Finally, using the optical band gap (E_g = 1.92 eV) determined from the UV-Vis DRS spectrum (Fig. S1a), the conduction band potential (E_{CB}) is estimated to be −0.92 V vs. NHE, according to the equation $E_{CB} = E_{VB} – E_g$. This energy level alignment confirms that the conduction band edge of MnO_2 is positioned at a more negative potential than the Zn^{2+}/Zn redox couple (−0.76 V vs. NHE), providing a strong thermodynamic driving force for the photo-reduction of Zn^{2+} ions.

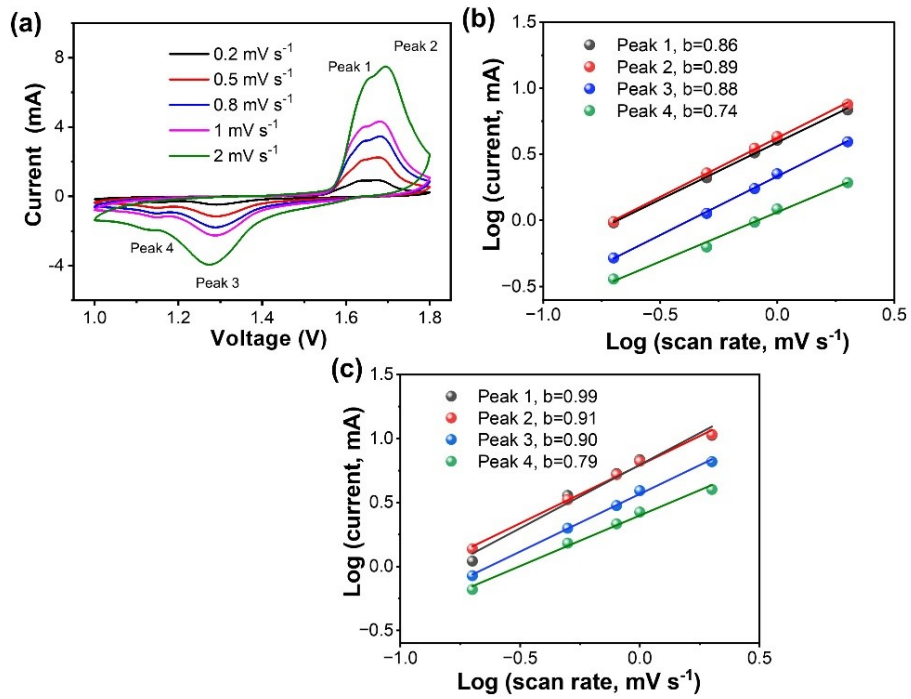

Fig. S2 (a) CV curves at different scan rates in the dark. Log(i) vs log (v) plots of four peaks in CV curves (b) in the dark and (c) under light irradiation.

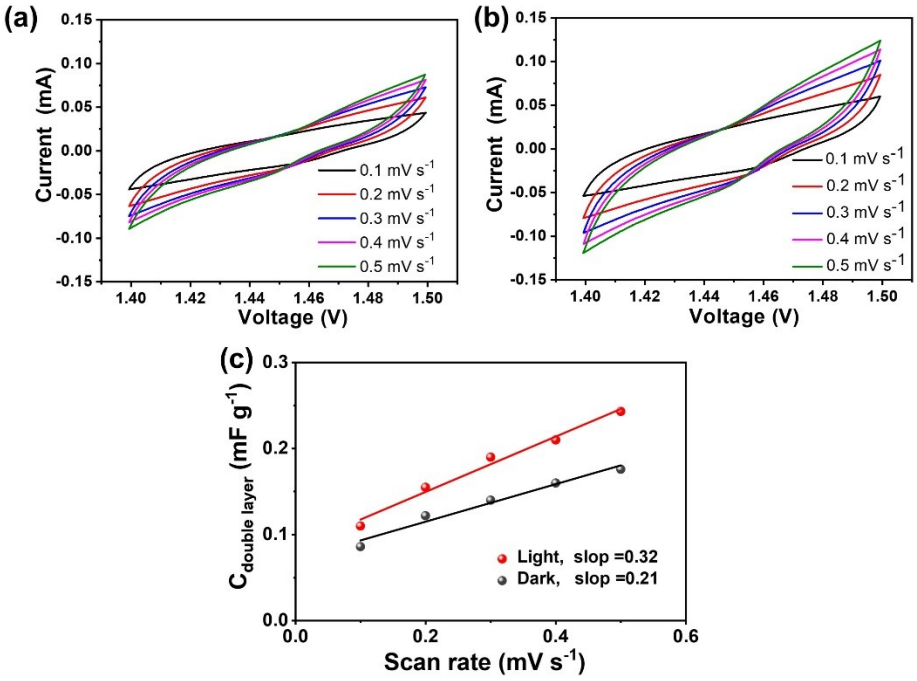

Fig. S3 CV curves of the photo-rechargeable ZIBs (a) in the dark and (b) under visible light irradiation and (c) their linear fit of current densities versus scan rates.

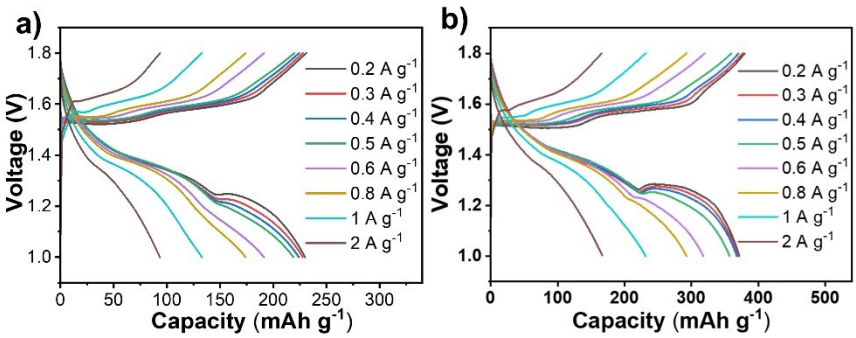

Fig. S4 Galvanostatic charge/discharge curves at different current densities (a) in the dark and (b) under light irradiation.

Table S1. Performance comparison of the reported photocathode and our materials.

Photocathode	Photo-charging voltage (V)	Photoconversion efficiency (%)	Ref.
VO_2/ZnO	0.88	0.51	[1]
MoS_2@TiO_2	0.91	0.7	[2]
VO_2/rGO	0.89	0.18	[3]
TiO_2@$CH_3NH_3PbI_3$	0.92	0.31	[4]
V_2O_5/P_3HT/rGO	0.95	1.2	[5]
V_2O_5/CdS	1.02	0.99	[6]
α-MnO_2/rGO	1.39	0.68	[7]
SnO_2@MnO_2	-	1.2	[8]
MoS_2/SnO_2/TiO_2@Ti	1.0	1.3	[9]
MnO_2/TiO_2	1.39	1.5	This work

References

[1] B. D. Boruah and M. D. Volder, *J. Mater. Chem. A,* 2021, **9**, 23199.

[2] T. Xiong, X. Zhou, Y. Wang, T. Zhou, R. Huang, H. Zhong, X. Zhang, S. Yuan, Z. Wang, J. Xin, J. Xue, W.S.V. Lee and L. Wei, *Energy Storage Mater*., 2024, **65**, 103146.

[3] B. D. Boruah, A. Mathieson, S. K. Park, X. Zhang, B. Wen, L. Tan, A. Boies and M. D. Volder, *Adv. Energy Mater*., 2021, **11**, 2100115.

[4] H. Liu, P. Wu, R. Wang, H. Meng, Y. Zhang, W. Bao and J. Li, *ACS Nano*, 2023, **17**, 1560.

[5] B. D. Boruah, A. Mathieson, B. Wen, S. Feldmann, W. M. Dose and M. D. Volder, *Energ. Environ. Sci*., 2020, **13**, 2414.

[6] J. Liu, Y. Wang, G. Li, A. Fu, J. Fan, S. Cong, L. Wang, S. Zhang, X. Xie and N. Zhang, *Small*, 2026, https://doi.org/10.1002/smll.202512983.

[7] Z. Zheng, C. Ding, M.S. Hasan, K. Wang, Y. Liu, W. Yang, J. Cheng, Z. Luo, S. Cao and Y. Ding, *Adv. Funct. Mater*., 2025, **35**, 2500182.

[8] X. Gao, D. Tian, Z. Shi, N. Zhang, R. Sun, J. Liu, H.-S. Tsai, X. Xiang and W. Feng, *Small*, 2024, **20**, 2405627.

[9] D. Yang, C. Xin, W. Zhang, H. Liu, F. Gao, S. Dou and T. Xiong, *Chem. Eng. J*., 2026, **531**, 173997.